Applied Thermal Engineering 102 (2016) 1481–1491

Contents lists available at ScienceDirect

Applied Thermal Engineering

journal homepage: www.elsevier.com/locate/apthermeng

Research Paper

Heat transfer and friction characteristics of shell and tube heat exchanger with multi inserted swirl vanes

Mahmoud Galal Yehia [a,*], Ahmed A.A. Attia [b], Osama Ezzat Abdelatif [b], Essam E. Khalil [c]

[a] Mechanical Power Engineering, Faculty of Engineering at Shoubra, Benha University, Egypt
[b] Department of Mechanical Engineering, Faculty of Engineering at Shoubra, Benha University, Egypt
[c] Department of Mechanical Power Engineering, Faculty of Engineering, Cairo University, Cairo, Egypt

HIGHLIGHTS

- Higher vane swirlers diameter and blade angle give the best results.
- Heat transfer increases with increasing number of inserted vane swirlers.
- Thermal enhancement factor increase with increasing inserted vane swirlers.
- Six inserted vane swirlers gives the maximum heat transfer enhancement.
- Obtain a correlation for heat transfer and friction with multi inserted vane swirlers.

ARTICLE INFO

Article history:
Received 15 September 2015
Accepted 14 March 2016
Available online 25 March 2016

Keywords:
Numerical simulation
Shell and tube heat exchanger
Turbulence model
Swirl vane

ABSTRACT

The effect of friction characteristics of the heat exchanger model when using different number of swirl vanes at different locations along the pipe length to enhance the heat transfer rate will be discussed through a simulation for shell and tube heat exchanger using ANSYS FLUENT CFD techniques. The number of swirl vanes inserted into each tube is three swirl vanes and six swirl vanes distributed along the pipe length with variable diameter (10 mm, 15 mm, 19 mm) and different blade angle (15°, 30°, 45°) for each case. The results show that the numerical results reasonably agree well with the available literature. The case of six swirl vanes with 19 mm diameter and 45° blade angle gives the maximum heat transfer enhancement, friction factor, and thermal enhancement factor compared with plain tube case. A correlation for Nusselt number and friction factor is developed.

1. Introduction

Heat exchangers are found in the power generation field and in numerous industrial applications. The shell and tube heat exchangers are the most versatile types of heat exchangers and it is the most widely used in these fields. That is due to their relatively simple construction and the multi-purpose application possibilities for fluid media in a very large temperature and pressure range. This has led to increase the levels of research on the heat transfer and hydraulic behavior of heat exchangers experimentally, analytically and numerically [1].

Many parameters affecting the design of heat exchangers, including thermal analysis, weight, size, pressure drop, and cost. Economics plays a key role in the design and selection of heat exchangers equipment. The weight and size of heat exchangers are significant parameters in the overall application and thus may still be considered as variables involved in economic evaluation. Another crucial issue in designing and sizing any type of heat exchange device is the calculation of convective heat transfer coefficients. Thus, its correct determining permits for the proper selection of heat transfer area during designing of heat exchangers and calculation of the fluid outlet temperature. A lot of efforts have been made during experimental investigations of pressure drop and heat transfer in different types of heat exchangers to obtain proper heat transfer correlation formulas [2].

An earlier study of the present authors; the first study of Yehia et al. [3] was focused on obtaining a numerical model capable of predicting heat transfer and friction characteristics for shell and tube heat exchanger through selecting the proper mesh density, turbulence model, and validating the resultant model with the available relevant analytical, experimental, and numerical literature. The second study of Yehia et al. [4] was focused on maximizing heat transfer and minimizing friction loss in the previous

* Corresponding author.
E-mail addresses: medogalal@yahoo.com (M.G. Yehia), ahmed.attia@feng.bu.edu.eg (A.A.A. Attia), osama.abdellatif@feng.bu.edu.eg (O.E. Abdelatif), khalile1@asme.org (E.E. Khalil).

http://dx.doi.org/10.1016/j.applthermaleng.2016.03.095
1359-4311/

Nomenclature

A	area (m^2)
c_p	pressure coefficient (J/(kg K))
$C_{1\varepsilon}$	constant
$C_{2\varepsilon}$	constant
$C_{3\varepsilon}$	constant
D	diameter (m)
D_b	propeller diameter (m)
D_p	pipe diameter (m)
f	friction factor
G_b	generation of turbulent kinetic energy due to buoyancy (m^2/s^2)
G_k	turbulent kinetic energy production (m^2/s^2)
h	heat transfer coefficient (W/(m^2 K))
h_i	heat transfer coefficient for pure cross flow in ideal tube bank (W/(m^2 K))
J_c	segmental baffle window correction factor
J_l	baffle leakage correction factor
J_b	bypass correction factor, tube bundle to the shell
J_s	unequal inlet/outlet baffle spacing correction factor, apply only if such differences exist
J_r	laminar heat transfer correction factor, applicable for $Re < 100$
k	turbulence kinetic energy (m^2/s^2)
L	length (m)
L_p	pipe length (m)
L_t	inter-turbulator distance (m)
$\dot{m}$	mass flow rate (kg/s)
na	constant
Nu	Nusselt number
p	pressure (Pa)
Pr	Prandtl number
Re	Reynolds number
S_k	user-defined source term
S_ε	user-defined source term
t	time (s)
T	temperature (K)
TEF	thermal enhancement factor
u	velocity (m/s)
U	the mean velocity near the wall region (m/s)
Y_M	the dilatation dissipation term
x, y, z	Cartesian coordinate Component
u, v, w	instantaneous velocity component in x, y, z directions
Δp	pressure drop between inlet and outlet (Pa)
Δp_c	combined pressure drop of all the interior cross flow section (baffle tip to baffle tip) (Pa)
Δp_w	combined pressure drop in all the windows crossed (Pa)
Δp_e	pressure drop in the two end zones (Pa)
ΔT	temperature difference (K)
α_ε	inverse effective Prandtl numbers for the turbulent kinetic energy
α_k	inverse effective Prandtl numbers for the dissipation
ρ	density (kg/m^3)
μ	dynamic viscosity (kg/(m s))
κ	thermal conductivity (W/(m K))
ε	dissipation rate
θ	blade angle (°)
φ	swirl fan diameter (mm)
ω	specific dissipation rate (s^{-1})

Subscripts and superscripts

av	average
b	bulk (i.e., mathematical average between inlet and outlet)
D	diameter
m	mean
Pl	plain tubes
s	shell side
sr	surface
t	tube side
v	tubes with inserted swirl vanes
eff	effective property
i, j, k	donates Cartesian coordinates direction takes the value of axis X, Y, Z
$-$	mean property or time average
$'$	fluctuating component of any property

Abbreviations

CFD	computational fluid dynamics
RNG	renormalization group
RSM	Reynolds-stress model
SST	shear-stress transport

heat exchanger model by inserting single swirl vane in the inlet of each tube with variable vane diameter and blade angle. While, the objective of the present study focused on inserting multi swirl vanes per each tube to increase the heat transfer enhancement and avoid the high levels of friction loss associated when using single swirl vane. The aim of using swirl vane is as a heat transfer enhancement device for decreasing the weight and size to obtain the most possible cost reduction.

2. Literature survey

2.1. Experimental investigations

The experiments, primary concern on the determination of overall heat transfer coefficient and Nusselt number as a direct index on heat exchanger performance. Also, one of their concerns is to determine the pressure drop and friction factor at different geometric arrangements.

Kurtbas et al. [5], have investigated experimentally the effect of freely rotating propeller-type turbulators with variable angle (θ), diameter (D_b) and number of blades located in the inner pipe of a counter flow double pipe heat exchanger on heat transfer (Nu) of turbulent air flow at a Reynolds number range from 10^4 to 3×10^4, and developing the corresponding empirical correlations for Nusselt number as follows:

$$Nu = 0.343Re^{0.62}(1 + \tan\theta)^{-1.006} \times (D_b/D_p)^{0.625}(L_t/L_p)^{-0.336} \quad (1)$$

where the correlation range is θ = 10°, 20° and 40°, D_b/D_p = 0.8, 0.83 and 0.87 and Re = 10,000–30,000.

The main conclusions from this investigation are as follows:

- Maximum decaying distance of swirl flow was found to be one third of pipe length.
- Lower blade angle and minimum inter-turbulator distance (L_t/L_p) gives higher efficiency.
- Nusselt number increases with the decrease in blade angle and inter-turbulator distance, and with the increase in Reynolds number.
- Nusselt number with propeller type turbulator increases about 3.6 times that of plain pipe.

Eiamsa-ard et al. [6] have investigated experimentally the effect of regularly-spaced dual twisted tapes with variable twist and space ratios in comparison with single and dual full-length twisted

tapes. The tapes located in a uniform wall heated pipe. Heat transfer and friction characteristics of turbulent air flow at a Reynolds number range from 4000 to 19,000 are investigated. An empirical correlation for Nusselt number and friction factor of a plain tube case are developed as:

$$Nu = 0.017Re^{0.82}Pr^{0.4} \quad (2)$$

$$f = 3.1Re^{-0.48} \quad (3)$$

Thianpong et al. [7] have investigated experimentally the effect of twisted tape with variable twist ratio, in a dimpled inner pipe of a counter flow double pipe heat exchanger with dimple variable pitch ratio. Heat transfer and friction characteristics of turbulent air flow at a Reynolds number range from 12,000 to 44,000 are investigated. An empirical correlation for Nusselt number and friction factor of the inner plain tube case are also given as:

$$Nu = 0.049Re^{0.706}Pr^{0.4} \quad (4)$$

$$f = 0.718Re^{-0.309} \quad (5)$$

2.2. Analytical investigations

In the present investigation, it was found that the analytical methods with its corresponding empirical correlations of heat transfer and friction have limitations and are of doubtful accuracy.

For the tube side flow's friction correlations, Blasius [8] correlation in fully developed turbulent flow as follows.

$$f = 0.316Re^{-0.25} \quad \text{For } Re \leqslant 2 \times 10^4 \quad (6)$$

$$f = 0.184Re^{-0.2} \quad \text{For } Re \geqslant 2 \times 10^4 \quad (7)$$

Petukhov correlation [9] for fully developed turbulent flow at $3000 \leqslant Re \leqslant 5 \times 10^6$ is given as:

$$f \equiv (0.790 \ln Re - 1.64)^{-2} \quad (8)$$

For the tube side flow's heat transfer correlations, Colburn correlation [10] for fully developed (hydro-dynamically and thermally) turbulent flow in a smooth circular tube is given as:

$$Nu = 0.023Re^{4/5}Pr^{1/3} \quad (9)$$

The Dittus–Boelter equation [11] for fully developed turbulent flow is given as:

$$Nu_D = 0.023Re_D^{4/5}Pr^{na} \quad (10)$$

where na = 0.4 for heating ($T_{sr} > T_m$) and 0.3 for cooling ($T_{sr} < T_m$), for the range of conditions $0.6 \leqslant Pr \leqslant 160$, $Re_D \geqslant 10{,}000$, $L/D \geqslant 10$.

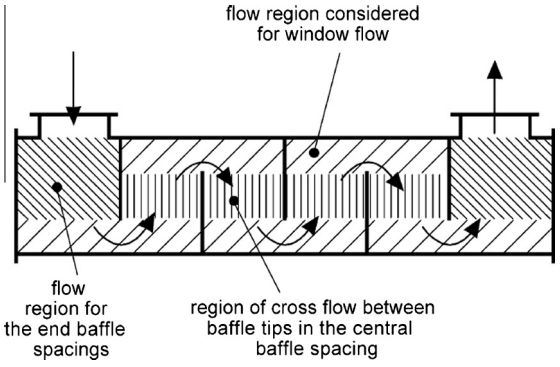

Fig. 1. The three components of the pressure drop (Δp_c, Δp_w, Δp_e) referred to the three flow zones [13].

For the shell side flow, Bell-Delaware [12] method, the heat-transfer coefficient and pressure drop are estimated from correlations to flow over ideal tube-banks, and the effects of leakage, bypassing and flow in the window zone are allowed for by applying correction factors. Bell-Delaware method assumes that the flow rate and the thermo-physical properties of the shell-side fluid are specified; also shell-side geometrical parameters are known.

The correlation for shell-side heat transfer coefficient is [12]:

$$h_s = h_i(J_c J_l J_b J_s J_r) \quad (11)$$

where h_s is the shell side heat transfer coefficient, h_i is the heat transfer coefficient for pure cross flow in the ideal tube bank, J_c is the segmental baffle window correction factor, J_l is the baffle leakage correction factor, J_b is the bypass correction factor, tube bundle to shell, J_s is the unequal inlet/outlet baffle spacing correction factor, applicable only if such differences exist and J_r is the laminar heat transfer correction factor, applicable for $Re < 100$.

The correlation for shell-side pressure drop is [12]:

$$\Delta p_s = \Delta p_c + \Delta p_w + \Delta p_e \quad (12)$$

where as shown in Fig. 1, Δp_s are the total shell-side pressure drop excluding nozzles, Δp_c is the combined pressure drop of all the interior cross flow section (baffle tip to baffle tip), Δp_w is the combined pressure drop in all the windows crossed and Δp_e is the pressure drop in the two end zones.

As a general conclusion, it can be said that correlation based approaches may indicate the existence of a weakness in the design, but CFD simulations can also pinpoint the source and the location of the weakness. Using CFD, together with supporting experiments, may speed up the shell-and-tube heat exchanger design process and may improve the quality of the final design.

2.3. Numerical investigations

Ozden and Tari [14] have investigated numerically using the commercial CFD package FLUENT 6.3, the dependencies of the shell side geometrical parameters. The number of baffles of 6, 8, 10, and 12, baffle cut ratio of 25% and 36% on the shell side heat transfer coefficient and the pressure drop at different shell side mass flow rate of 0.5, 1.0, and 2.0 kg/s. Water is the shell side working fluid with inlet temperature of 300 K, and a constant tube wall temperature of 450 K.

The shell size with inner diameter of 90 mm, length of 600 mm, tubes, outer diameter of 20 mm, tube bundle geometry and pitch are triangular of 30 mm, number of tubes are 7 and the main conclusions of this investigation are as follows:

The k–ε realizable turbulence model with first order discretization and the fine mesh of 1,360,000 elements is selected as the best simulation approach. For this heat exchanger geometry; 25% baffle cut gives slightly better results. Increasing the number of baffles would improve the heat transfer characteristics of the heat exchanger.

Also, Ur-Rehman [15] has investigated numerically using FLUENT, the heat transfer coefficient and pressure drop of a unbaffled shell-and-tube heat exchanger and concluded that k–ω SST model, with low Reynolds correction, provides better results as compared to other models.

Yehia et al. [3], have obtained a numerical model capable of predicting heat transfer and friction characteristics for shell and tube heat exchanger using ANSYS FLUENT, where the used model geometry was made typically as Ozden and Tari [14] and the main conclusions from this investigation are as follows:

- The number of cells of 2,132,064 cells relative to mesh volumes spacing internal size of 3, is the most robust and stable density.

– The RNG k–ε model with non-equilibrium wall functions and 2nd order upwind discretization found to be the best turbulence model for the investigated case.

Yehia et al. [4], have investigated numerically using ANSYS FLUENT the heat transfer and friction characteristics of turbulent water flow at mass flow rates of 0.5, 1.0, and 2.0 kg/s in the case of shell and tube heat exchanger as of Yehia et al. [3] but with single inserted swirl vane at 20 mm from the inlet of each tube with variable diameters of (5 mm, 10 mm, 15 mm, 18 mm, and 19 mm) and blade angles of (15°, 20°, 30°, 35°, 40°, 45°, and 60°), and developing the corresponding empirical correlations for Nusselt number as follows:

$$Nu = 0.2868\frac{(1+\tan\theta)^{0.0296}Re^{0.6187}f^{0.114}}{(D_b/D_p)^{0.0213}} \tag{13}$$

The main conclusions from this investigation are as follows:

– The insertion of a fixed swirl vane in the tube side; slightly affecting on the shell side Nusselt number and friction factor.
– The increase in mass flow rate; increases tube side Nusselt number, while slightly decreases the tube side friction factor and thermal enhancement factor.
– The increase in inserted swirl vane diameter with the decrease in blade angle; increases the tube side Nusselt number and friction factor, while decreases tube side thermal enhancement factor.
– The highest achieved heat transfer enhancement is for φ = 19 mm and θ = 15° case, resulting in, for Nusselt number, friction factor, and thermal enhancement factor times that of plain tubes case of 1.62, 58.75, and 0.42, respectively.

From the foregoing review, the three-dimensional numerical analysis of the thermal-hydraulic characteristics of the flow inside heat exchangers are still needed more modification and coordination. Most of the previous studies were focused on experimental way and developing the corresponding correlations. The main motivation of the present study was the low number of researches and the noticeable increase in heat transfer achieved in Yehia et al. [4], model, but with high levels of friction loss motivated the authors to present more development in this model to maximize heat transfer enhancement and decrease friction loss by inserting multi swirl vanes in each tube and investigate the proper number of swirl vanes, vane diameter, and blade angle that fit to the said target. Also, the present investigation will be accomplished numerically to reduce the high cost needed to use an actual size heat exchanger experimentally and to ensure the reliability of the obtained results will be verified with the available literature.

The following investigations are conducted on the case of inserting three vanes or six vanes in comparison with single vane that was obtained by Yehia et al. [4]. The studied cases are for vane diameters of 10 mm, 15 mm, and 19 mm, for blade angles of 15°, 30°, and 45°. The effect of these design parameters on heat transfer, friction factor, and the corresponding thermal enhancement factor will be presented. Finally, a trial to develop an empirical correlation between Nusselt number with friction factor, and compared with Kurtbas et al. [5] will be presented. Also, the corresponding relations between the heat transfer and friction factor will be presented.

3. Governing equations and turbulence model

3.1. Continuity equation

$$\frac{\partial u}{\partial x}+\frac{\partial v}{\partial y}+\frac{\partial w}{\partial z}=0 \tag{14}$$

3.2. Momentum equations

$$\rho\left(\bar{u}\frac{\partial\bar{u}}{\partial x}+\bar{v}\frac{\partial\bar{u}}{\partial y}+\bar{w}\frac{\partial\bar{u}}{\partial z}\right)=-\frac{\partial\bar{P}}{\partial x}+\mu\left(\frac{\partial^2\bar{u}}{\partial x^2}+\frac{\partial^2\bar{u}}{\partial y^2}+\frac{\partial^2\bar{u}}{\partial z^2}\right)-\rho\left(\frac{\partial\overline{(u')^2}}{\partial x}+\frac{\partial(\overline{u'v'})}{\partial y}+\frac{\partial(\overline{u'w'})}{\partial z}\right)\quad\text{in } x\text{-dir.} \tag{15}$$

$$\rho\left(\bar{u}\frac{\partial\bar{v}}{\partial x}+\bar{v}\frac{\partial\bar{v}}{\partial y}+\bar{w}\frac{\partial\bar{v}}{\partial z}\right)=-\frac{\partial\bar{P}}{\partial y}+\mu\left(\frac{\partial^2\bar{v}}{\partial x^2}+\frac{\partial^2\bar{v}}{\partial y^2}+\frac{\partial^2\bar{v}}{\partial z^2}\right)-\rho\left(\frac{\partial(\overline{u'v'})}{\partial x}+\frac{\partial\overline{(v')^2}}{\partial y}+\frac{\partial(\overline{v'w'})}{\partial z}\right)\quad\text{in } y\text{-dir.} \tag{16}$$

$$\rho\left(\bar{u}\frac{\partial\bar{w}}{\partial x}+\bar{v}\frac{\partial\bar{w}}{\partial y}+\bar{w}\frac{\partial\bar{w}}{\partial z}\right)=-\frac{\partial\bar{P}}{\partial z}+\mu\left(\frac{\partial^2\bar{w}}{\partial x^2}+\frac{\partial^2\bar{w}}{\partial y^2}+\frac{\partial^2\bar{w}}{\partial z^2}\right)-\rho\left(\frac{\partial(\overline{u'w'})}{\partial x}+\frac{\partial(\overline{v'w'})}{\partial y}+\frac{\partial\overline{(w')^2}}{\partial z}\right)\quad\text{in } z\text{-dir.} \tag{17}$$

3.3. Energy equation

$$\rho c_p\left(\bar{u}\frac{\partial\bar{T}}{\partial x}+\bar{v}\frac{\partial\bar{T}}{\partial y}+\bar{w}\frac{\partial\bar{T}}{\partial z}\right)=k\nabla^2\bar{T}-\rho c_p\left(\frac{\partial(\overline{u'T'})}{\partial x}+\frac{\partial(\overline{v'T'})}{\partial y}+\frac{\partial(\overline{w'T'})}{\partial z}\right) \tag{18}$$

$$\nabla^2\bar{T}\equiv\frac{\partial^2\bar{T}}{\partial x^2}+\frac{\partial^2\bar{T}}{\partial y^2}+\frac{\partial^2\bar{T}}{\partial z^2} \tag{19}$$

3.4. The RNG k–ε model

The RNG k–ε model was derived using a rigorous statistical technique (called renormalization group theory). It is similar in form to the standard k–ε model, but includes more features and refinements. These features make the RNG k–ε model more accurate and reliable for a wider class of flows than the standard k–ε model [16].

The transport equations for the turbulence kinetic energy k and its dissipation rate ε are:

$$\rho\frac{\partial k}{\partial t}+\rho U_i\frac{\partial k}{\partial x_i}=\frac{\partial}{\partial x_j}\left[\alpha_k\mu_{eff}\frac{\partial k}{\partial x_j}\right]+G_k+G_b-\rho\varepsilon-Y_M+S_K \tag{20}$$

$$\rho\frac{\partial\varepsilon}{\partial t}+\rho U_j\frac{\partial\varepsilon}{\partial x_j}=\frac{\partial}{\partial x_j}\left[\alpha_\varepsilon\mu_{eff}\frac{\partial\varepsilon}{\partial x_j}\right]+C_{1\varepsilon}\frac{\varepsilon}{k}(G_k+C_{3\varepsilon}G_b)-C_{2\varepsilon}\rho\frac{\varepsilon^2}{k}-R_\varepsilon+S_\varepsilon \tag{21}$$

4. Model configuration and Boundary conditions

The shell and tube heat exchanger model geometry presented in Fig. 2(a) was made exactly as Yehia et al. [3], were modeled. The selected model size and geometrical configuration match literature as in Refs. [3,4,14] to ease verification and enhancement investigation for the present study model. Also, it is found to be satisfactory for matching computational capabilities of the available computer hardware and the confidence in that the selected model size will generate significantly the same phenomenon in an actual size heat exchanger.

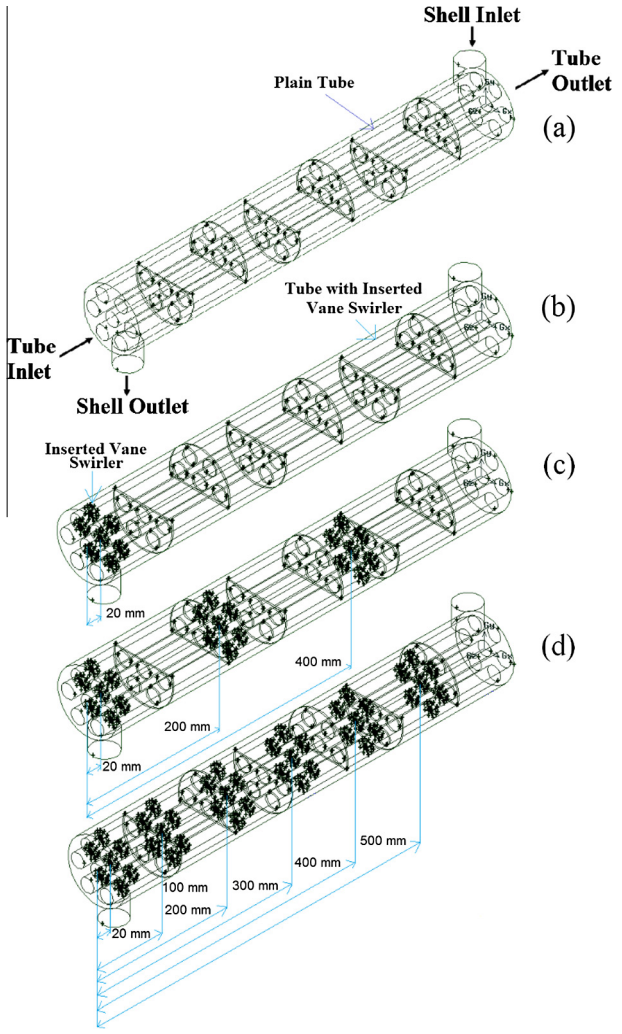

Fig. 2. Model configuration for (a) plain tube, case of Yehia et al. [3], (b) single inserted swirl vane, case of Yehia et al. [4], (c) three and (d) six inserted swirl vanes per each tube.

Table 1
Heat exchanger dimensions.

Description	Unit	Value
Shell diameter	mm	90
Shell inlet nozzle diameter	mm	36
Tube diameter	mm	20
Heat exchanger length	mm	600
No. of tube	–	7
Tube arrangement	–	60° Rotated triangular
No. of baffles	–	6
Baffle cut ratio	%	36

The main geometrical parameters are presented in Table 1. The effect of baffle clearance, and tube to baffle bypass leakages are neglected to ease the process of building such a model numerically, which is expected to not significantly affect on the present investigation's results compared to a real heat exchanger.

The inserted eight blade swirl vane, per each tube, is as in Fig. 3. The swirl vane diameter, blade angle, and location are varied as in Table 2 and as illustrated in Fig. 2(c) and (d) in comparison with Fig. 2(b) the case of inserting single swirl vane of Yehia et al. [4]. The detailed boundary conditions for the present study model are presented in Table 3.

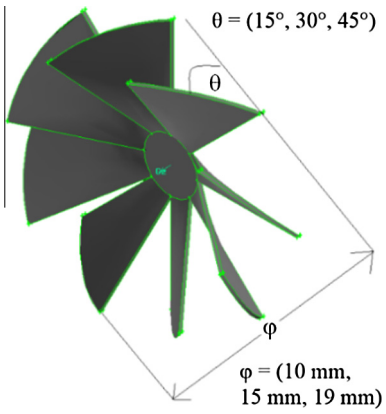

Fig. 3. Eight blades swirl vane geometry.

Table 2
Swirl vane geometry and location.

Swirl vane diameter (φ)	Swirl vane angle (θ)	Number of swirl vanes	Swirl vane number	Swirl vane position from tube side inlet
10 mm	15°	3	1	20 mm
			2	200 mm
15 mm	30°		3	400 mm
		6	1	20 mm
			2	100 mm
19 mm	45°		3	200 mm
			4	300 mm
			5	400 mm
			6	500 mm

5. Model solver parameters

The applied model solves many parameters as in Table 4 and the chosen turbulence model has been verified in an earlier investigation [3].

6. Heat transfer and friction calculations

The Nusselt number can be calculated as stated in Ref. [17] and it can be written as,

$$Nu = \frac{hD}{\kappa} \tag{22}$$

From the shell side, "h" is calculated from Eq. (11) as detailed in Ref. [10]. Along with ANSYS FLUENT model resultant temperatures and pressures, and from the tube side the following equation is applied,

$$h_t = \frac{\dot{m}_t c_{p,t} \Delta T_t}{A_{t,sr}(T_{t,w,av} - T_b)} \tag{23}$$

For tube side calculation D is calculated from tube diameter while in shell side calculation is calculated from the equivalent hydraulic diameter as detailed in Ref. [12]. κ and $c_{p,t}$ are calculated at the bulk temperature, $T_{t,w,av}$ is obtained from ANSYS FLUENT model.

The friction factor can be calculated as stated in Ref. [17]

$$f = \frac{\Delta p}{\frac{L}{D}\frac{\rho u^2}{2}} \tag{24}$$

Table 3
Model boundary conditions.

Description	Symbol	Unit	Value
Shell side			
Working fluid	–	–	Water
Inlet mass flow rate	$\dot{m}_s$	kg/s	0.5 1.0 2.0
Inlet Reynolds number	Re_s	–	10,290 20,370 40,740
Inlet temperature	$T_{s,i}$	K	350
Tube side			
Working fluid	–	–	Water
Total inlet mass flow rate	$\dot{m}_t$	kg/s	0.5 1.0 2.0
Inlet Reynolds number	Re_t	–	5318 10,637 21,274
Inlet temperature	$T_{t,i}$	K	300

Δp is obtained from ANSYS FLUENT model. While, ρ is calculated at the bulk temperature.

The main dimensionless parameter representing the relation between heat transfer and friction in tube side is the enhancement in heat transfer with respect to friction loss; is the thermal enhancement factor which can be calculated as stated in Ref. [18] and it can be written as follows:

$$TEF = \frac{(Nu_v/Nu_{pl})}{(f_v/f_{pl})^{1/3}} \quad (25)$$

7. Grid independence

Different mesh sizes have been used of 4,089,747, 2,132,064, 1,767,675, and 1,534,864 cells. The mesh size of 2,132,064 cells was the most suitable mesh size for the present study model as have been verified in an earlier investigation of Yehia et al. [3].

8. Turbulence model validation

Different models have been used in an earlier investigation of Yehia et al. [3] which are standard k–ε, RNG k–ε, Realizable k–ε, k–ω SST, and RSM. The 2nd order RNG k–ε model with non-equilibrium wall function and 2nd order pressure discretization scheme showed the best results compared to literature.

9. Shell and tube sides' validation

Shell and tube sides have been validated in an earlier investigation of Yehia et al. [3] which are briefly presented in this section as it is the same model used in the present study, but by adding multi swirl vanes per each tube. Main validation results are as follows:

- Tube side Nusselt number is validated with different correlations but deviates to a maximum percentage about 19.7% of the highest Reynolds number (Fig. 4a).
- Even though tube side friction factor predictions deviate in some cases up to 28.6%, the predictions are still considered satisfactory as it is laying between different correlations results (Fig. 4b).
- Even though the heat transfer coefficient and the pressure drop deviation reaches in some cases to 15.8% and 20%, respectively, the predictions are still considered satisfactory as it is laying between Ozden et al. [14] predictions and Bell-Delaware analytical method [12] (Fig. 5a and b).

10. Results and discussions

The process of heat transfer enhancement by using swirl vane is unavoidably accompanied by friction losses in the tubes with the increase in the required pumping power. As been concluded in Yehia et al. [4], the lower blade angle and higher swirl vane diameter generates friction losses within the heat exchanger of unsatisfactory level resulting in a low thermal enhancement factor. Consequently, in this section several attempts will be presented to generate higher heat transfer enhancement level from higher blade angles and lower swirl vane diameter without reaching high friction levels associated with lower blade angles and higher swirl vane diameter. One of the ways to reach this target is using multi swirl vanes have a high blade angle and small diameter. Accordingly, the cases of inserting three swirl vanes with geometries of ($\theta = 15°$, $\varphi = 10$ mm), ($\theta = 30°$, $\varphi = 15$ mm) and ($\theta = 45°$, $\varphi = 19$ mm) and inserted six swirl vanes with the same geometries will be studied and will be presented in comparing with two cases, the plain tube case that was previously studied by Yehia et al. [3], and single swirl vane case as of Yehia et al. [4]. Finally a conclusion with the optimum case will be presented.

10.1. Heat transfer for multi inserted swirl vanes per each tube

The main factors affecting on heat transfer as can be found in Eq. (23) are the heat transfer area, temperature difference and flow rate. The heat transfer area is fixed in the present investigation. The insertion of swirl vanes along the tube length induces swirling flow which works to greatly intensify the fluid mixing and boundary layer disturbing. This is due to the strengthening of the near-wall swirling when flow passing through each of the inserted vane swirlers and the temperature gradient becomes larger in the boundary layer simultaneously. Therefore, convective heat transfer will be substantially enhanced and the outlet temperature will be higher as will be discussed in the next paragraph. While this enhancement effect on heat transfer increases with the increase in mass flow rate due to the increase in turbulence intensity.

The Nusselt number ratio for heat exchangers for single, three, and six swirl vanes per each tube with similar blade angle and vane diameter in the case of $\varphi = 10$ mm and $\theta = 15°$ is presented in Fig. 6.

Table 4
Model solver parameters.

Item		Type
Thermo-physical properties between inlet hot and cold fluids		Piecewise-linear profile
Shell and tube sides	Inlet conditions	Velocity-inlet type
	Outlet conditions	Pressure-outlet type
Turbulence model		RNG k–ε with non-equilibrium near-wall treatment functions.
Under-relaxation factors		FLUENT defaults except energy and turbulent viscosity of 0.8
Pressure–velocity coupling		SIMPLE
Discretization schemes		2nd order upwind

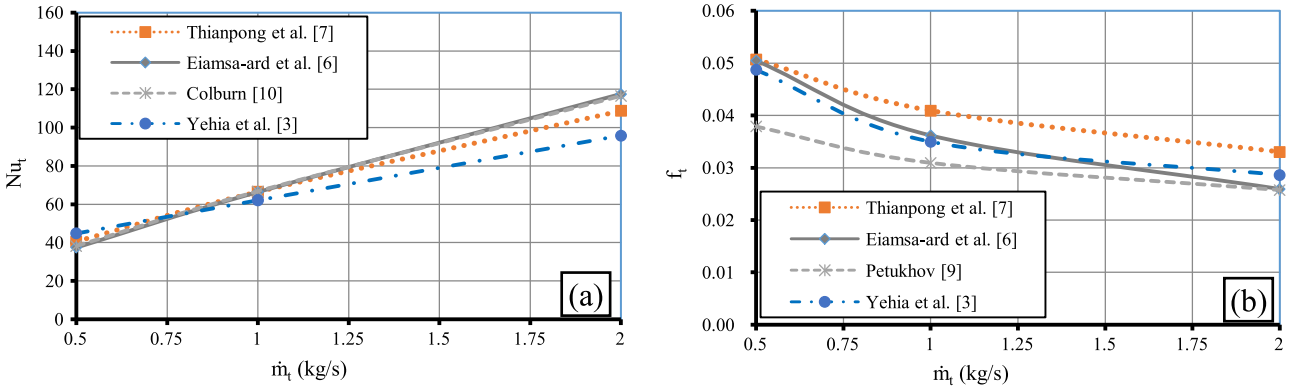

Fig. 4. Predictions of Yehia et al. [3] for tube side Nusselt number and friction factor in comparison with Thianpong et al. [7], Eiamsa-ard et al. [6], Colburn [10] and Petukhov [9] correlations.

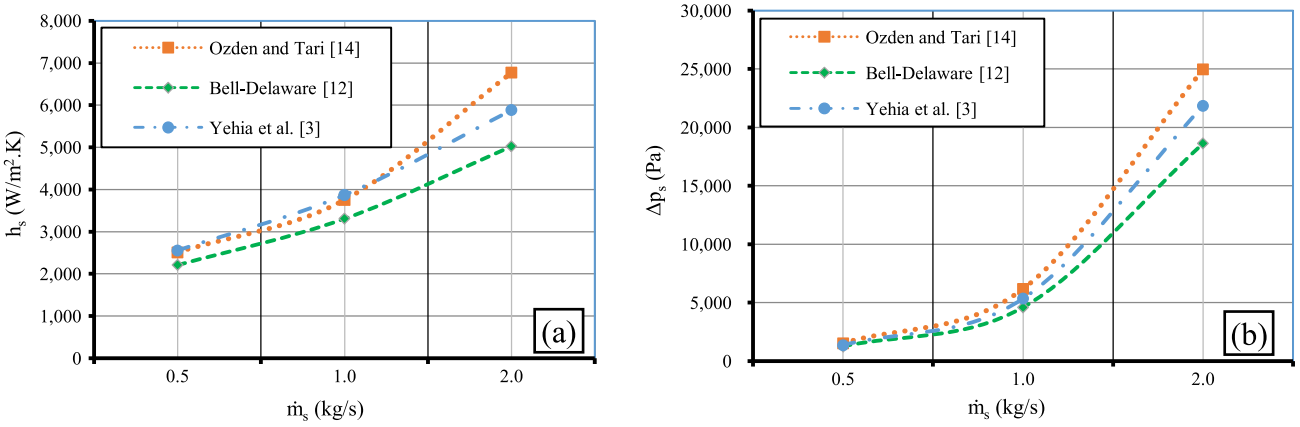

Fig. 5. Predictions of Yehia et al. [3] for shell side heat transfer coefficient and pressure drop in comparison with Ozden and Tari [14] predictions and Bell-Delaware [12] correlation.

The results show that increasing numbers of swirl vanes increase heat transfer enhancement to a maximum level, about 38% for six inserted swirl vanes. This leads to conclude that increasing numbers of insertion swirl vanes will increase heat transfer enhancement when fluid pass to the next vane due to the re-intensifying the turbulence intensity which consequently increases fluid mixing between hot and cold fluids leading to decreases the thermal boundary layer thickness. In the case of swirl vane (φ = 19 mm and θ = 45°) in Fig. 6(c) the maximum heat transfer enhancement is about 130% when six swirl vanes were used. Fig. 6(a), (b) and (c) shows that even though decreasing blade angle increases Nusselt number, the increase in swirl vane diameter gives higher effect on the resultant Nusselt number than the decrease in blade angle, resulting in with φ = 19 mm and θ = 45° is giving the maximum heat transfer enhancement of 82% and 130% for the cases of three and six inserted swirl vanes per each tube respectively, which can be useful in maximizing heat transfer with lower friction level from using lower blade angle.

10.2. Friction factor for multi inserted swirl vanes per each tube

The main factors affecting the pressure drop appearing from Eq. (24) are the fluid density, flow passage area, friction factor and fluid velocity. The fluid density is extracted from fluid thermo physical properties. The flow passage area is fixed in the present investigation. The insertion of swirl vanes along tubes length increase fluid mixing and boundary layer disturbing which increases flow resistance and velocity inside tubes. Thus, the flow boundary layer becomes thinner and this will result in a significant increase in pressure drop and consequently in the friction factor as will be discussed in the next paragraph. While the friction loss increases with the increase in fluid velocity due to the increase in the effect of flow blockage from swirl vanes with the increase in fluid velocity.

The tube side friction factor ratio for heat exchangers with single, three, and six inserted swirl vanes per each tube with similar blade angle and vane diameter in the case of φ = 10 mm and θ = 15° show that increasing numbers of swirl vane increases the friction factor to a maximum level for six inserted vanes of 5.3 times that of plain tubes as shown in Fig. 7(a). This is due to the increase in flow blockage and turbulence intensity combined with the increase in number of swirl vanes in flow passage which increases both heat transfer and friction. Increasing both vane diameter and blade angle for the case of φ = 15 mm and θ = 30° in Fig. 7(b) maximum friction factor is for six inserted vanes of 17.2 times that of plain tubes. For the case of φ = 19 mm and θ = 45° in Fig. 7(c) maximum friction factor is for six inserted vanes of 19 times that of plain tubes.

Fig. 7(a), (b) and (c) shows the same behavior of heat transfer that was discussed in the previous section. Even though decreasing blade angle increase friction factor, the increase in swirl vane diameter gives higher effect on the resultant friction factor than the decrease in blade angle. Resulting in with φ = 19 mm and θ = 45° gives the maximum friction factor of 12.04 and 19 times that of plain tubes friction factor, in the cases of three and six swirl vanes per each tube respectively.

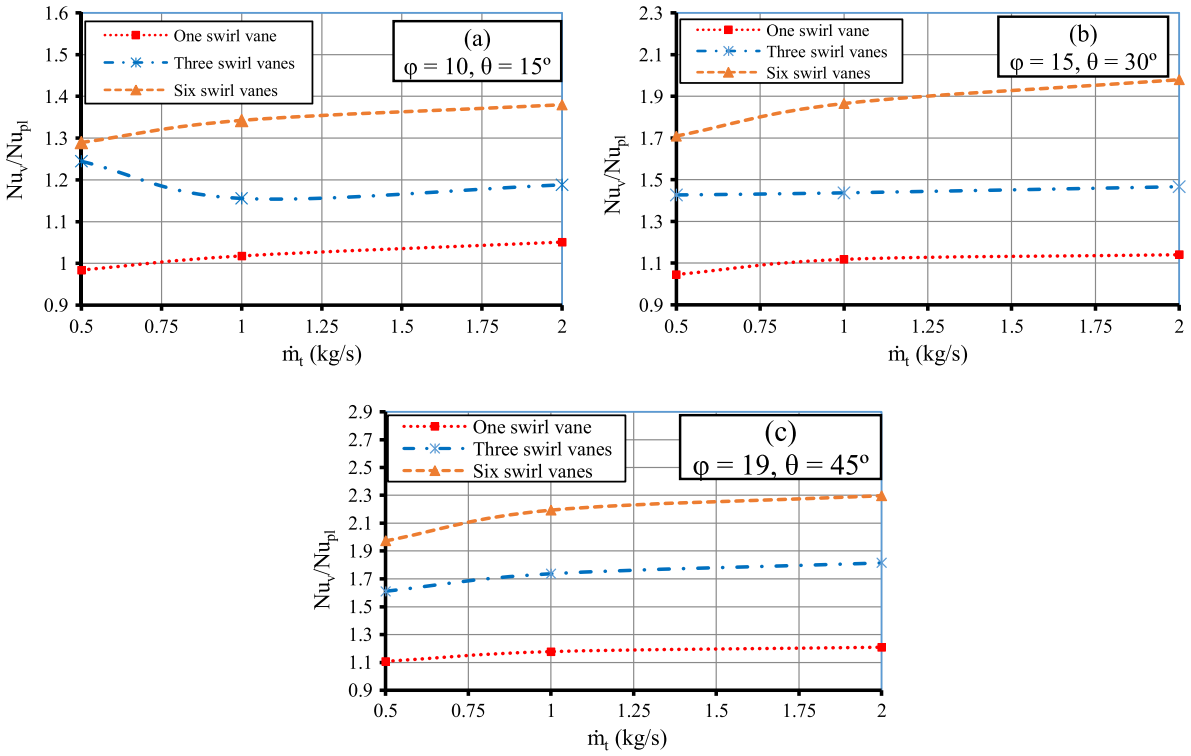

Fig. 6. Tube side Nusselt number ratio vs. mass flow rate for single, three and six inserted swirl vanes at different diameter (φ = 10, 15, 19 mm) for different swirl angle (θ = 15°, 30°, 45°).

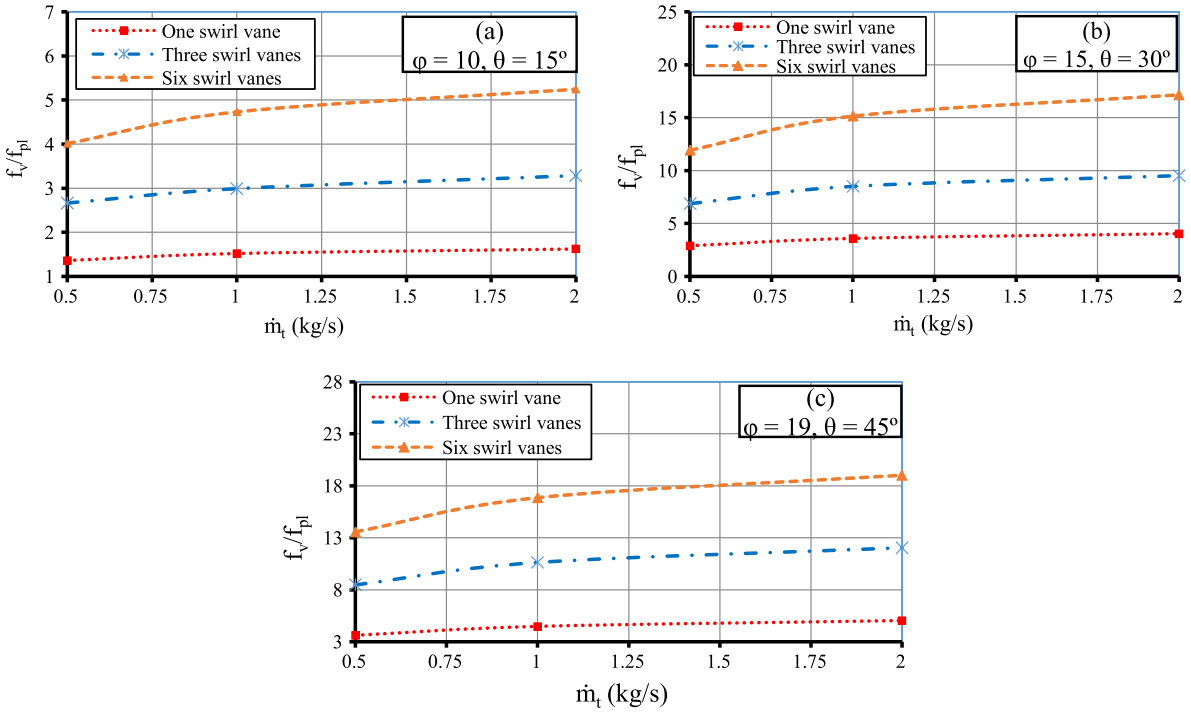

Fig. 7. Tube side friction factor ratio vs. mass flow rate for single, three and six inserted swirl vanes at different diameter (φ = 10, 15, 19 mm) for different swirl angle (θ = 15°, 30°, 45°).

10.3. Correlation for multi inserted swirl vanes per each tube

The present predictions for Nusselt number and friction factor are presented in a correlation using a regression method with a standard deviation of 4.0%, and the correlation is as follows:

$$Nu = 0.265\frac{(1+\tan\theta)^{0.143}Re^{0.626}f^{0.145}}{(D_b/D_p)^{0.049}(L_t/L_p)^{0.167}} \quad (26)$$

where the correlation range is θ = 15°, 30°, and 45°, D_b/D_p = 0.5, 0.75, and 0.95, L_t/L_p = 1, 0.333, and 0.167 at Re = 5000–21,000.

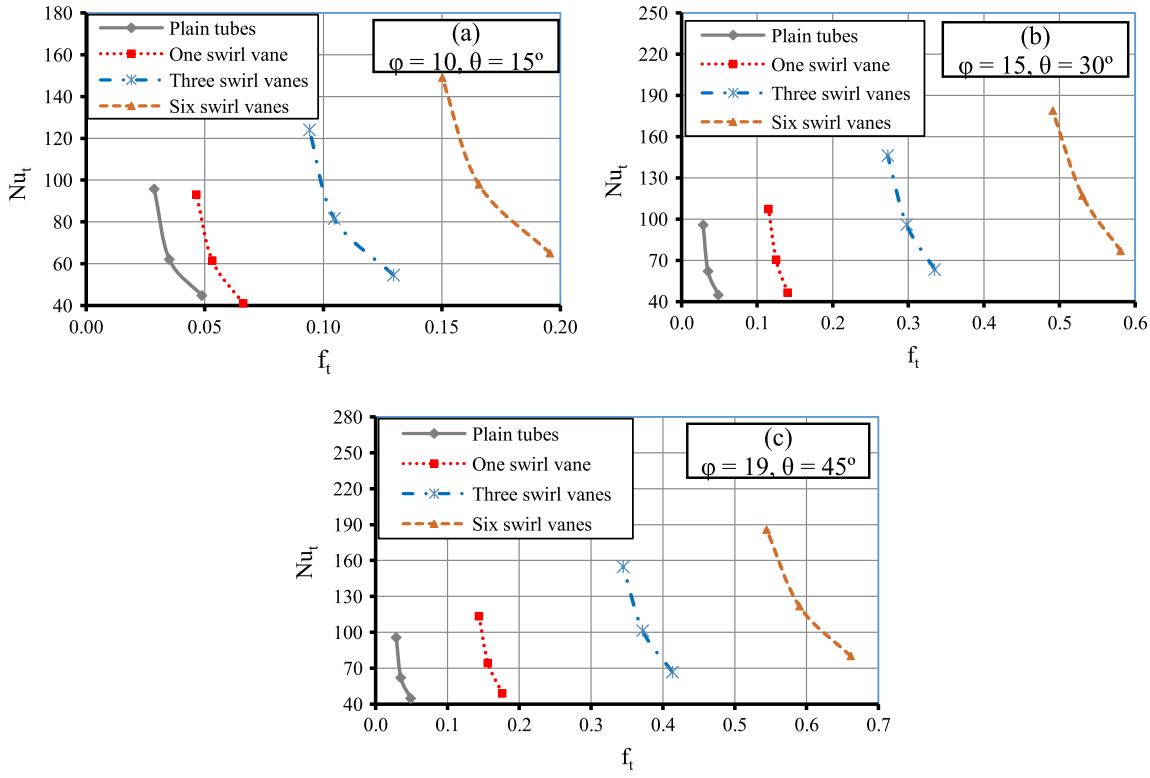

Fig. 8. Tube side Nusselt number vs. friction factor for plain tubes and single, three and six inserted swirl vanes at different diameter (φ = 10, 15, 19 mm) for different swirl angle (θ = 15°, 30°, 45°).

The above defined variable input values for θ, D_b/D_p, L_t/L_p, Re and the resultant values for Nu and f obtained from solving Eqs. (22) and (24) are collected in a table and using regression analysis in Microsoft Excel putting Nu values as the input Y range and θ, D_b/D_p, L_t/L_p, Re, f as input X's range then this data analyzer will derive the coefficients for the said X variables which consequently forms Eq. (26).

The effect of using plain tubes and single or three or six swirl vanes with different blade angles (θ = 15°, 30° and 45°) and swirl vane diameters of (φ = 10 mm, 15 mm and 19 mm) on the relation between Nusselt number and friction factor is shown in Fig. 8(a), (b) and (c). It is clear that the increase in the Nusselt number decreases the friction factor and this effect is decreased with the increase in swirl vane diameter and the values for both are increased with the decrease in blade angle and the effect of blade angle are more significant with the increase in swirl vanes' diameter. Also, the increase in friction factor in more noticeable than the increase in Nusselt number with the increase in number of inserted swirl vanes due to higher fiction levels compared to heat transfer enhancement.

10.4. Comparison with others' results for multi inserted swirl vanes per each tube

In continuing to the validation study made in Yehia et al. [3] and briefly presented in validation section, so a comparison to the case of multi inserted swirl vanes is made between the Kurtbas et al. [5] correlation, the present predictions, and the present correlation for the range that considerably close to Kurtbas et al. [5] correlation as shown in Fig. 9(a) and (b). The comparison shows the same trend for relation curve between tube side Nusselt number and Reynolds number which give a more confidence in both present predictions and the developed correlation.

10.5. Thermal enhancement factor for multi inserted swirl vanes per each tube

The evaluation of potential for real application of the inserted fixed swirl vanes as heat transfer enhancement device is performed using thermal enhancement factor. In general, a friction factor ratio increases with increasing Reynolds number. Conse-

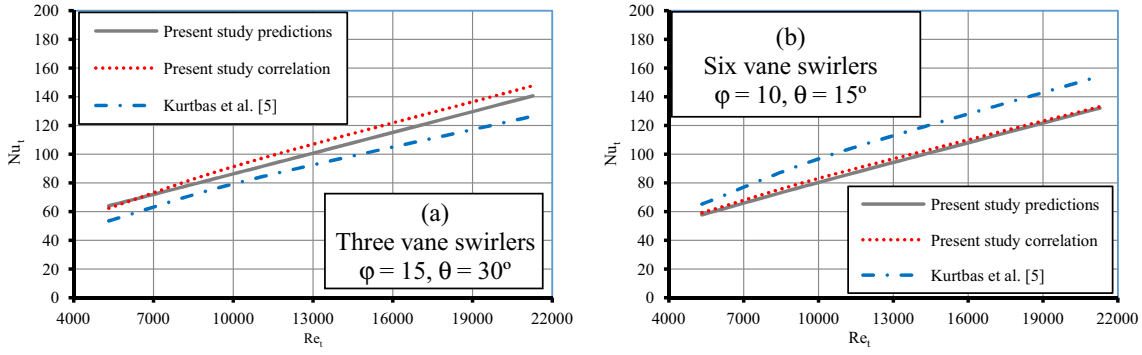

Fig. 9. Tube side Nusselt number vs. Reynolds number for three and six inserted swirl vanes at different φ (15, 10 mm) and θ (30°, 15°).

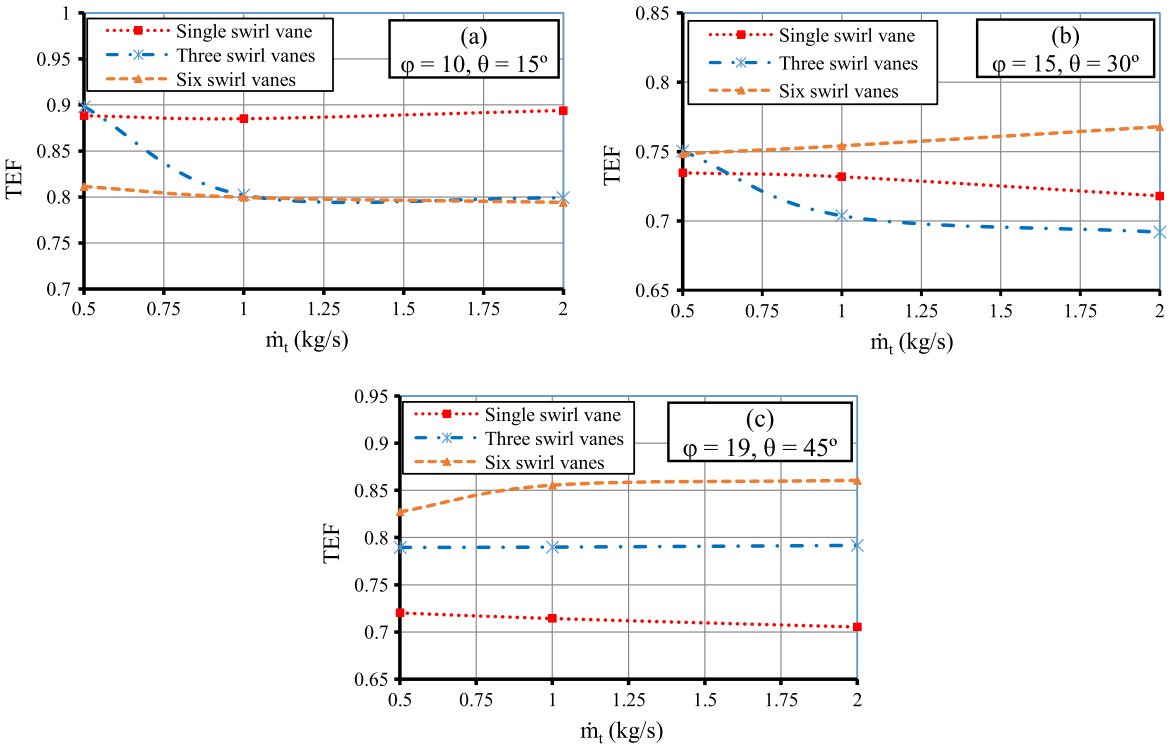

Fig. 10. Tube side thermal enhancement factor vs. flow rate for single, three and six inserted swirl vanes at (φ = 10 mm, θ = 15°), (φ = 15 mm, θ = 30°) and (φ = 19 mm, θ = 45°).

quently, the effect of a friction factor ratio becomes dominantly over the Nusselt number ratio at high Reynolds number (turbulent flow regime), resulting in thermal performance less than unity. On the other hand, the thermal enhancement factors above unity are in low Reynolds number regime (laminar flow regime), indicating the potential of these inserted swirl vane as energy-saving devices as in all cases of swirling flow, the heat transfer increased at the expense of an increase in pressure drop.

Swirl vanes insertion means a decrease in the flow passage area and creating a swirl flow, which provides more contact between the fluid and the tube wall, resulting in higher velocity and temperature gradient in the tube side, hence the higher pressure drop and higher heat transfer. Consequently, an increasing number of swirl vanes reduce TEF as the pressure drop is higher than the gained heat transfer as seen in Fig. 10(a) for the case of φ = 10 mm and θ = 15°. But with increasing both blade angle and vane diameter the friction values, increases, but at a lower level than the increase in heat transfer as in Fig. 10(b) and (c) which means that the higher number of inserted swirl vanes with higher blade angle and vane diameter is the most efficient heat transfer enhancement device. Consequently, the case of six inserted swirl vanes per each tube at φ = 19 mm and θ = 45° gives a maximum valve for TEF of 0.79 and 0.86 for the cases of three and six inserted swirl vanes per each tube respectively, which means that the case of six inserted swirl vanes is the most achieved efficient enhancement devices in the present study.

11. Conclusions

CFD model was developed and tested for validation and agreement with other authors' results leads to simulate the flow fields across heat exchangers over a wide range of flow temperatures, Reynolds numbers, and geometry configurations.

Many important predictions were revealed in this research, which demonstrate some important conclusions:

- The increase in mass flow rate; increases tube side Nusselt number, tube side friction factor while slightly decreases thermal enhancement factor.
- The increase in inserted vane swirlers diameter with the decrease in blade angle; increases the tube side Nusselt number and friction factor, while decreases tube side thermal enhancement factor.
- The three swirl vanes have a highest achieved heat transfer enhancement at φ = 19 mm and θ = 45° case. The resulting Nusselt number, friction factor, and thermal enhancement factor times that of plain tubes case of 1.82, 12.04, and 0.79, respectively.
- The six swirl vanes have a highest achieved heat transfer enhancement at φ = 19 mm and θ = 45° case. The resulting Nusselt number, friction factor, and thermal enhancement factor times that of plain tubes case of 2.3, 19.02, and 0.86, respectively.
- The multi inserted swirl vanes with higher diameter and blade angle is better in heat transfer enhancement, friction factor, and thermal enhancement factor than using a single inserted swirl vane with high swirl vane diameter and low blade angle.
- An increasing in number of inserted swirl vanes enhances heat transfer and thermal enhancement factor which means a more efficient heat exchanger with lower heat transfer area and volume and consequently a lower cost.
- The case of six inserted swirl vanes with φ = 19 mm and θ = 45° is found to be the superior case for achieving the maximum heat transfer enhancement with moderate levels of friction.
- The presented swirl vanes are very easy to be manufactured. These vanes could be assembled in tubes through welding to tube inner walls using special welding torch and to be assembled sequentially starting with the inner most till assembling the last vane at the tube inlet. Also, these swirl vanes can be assembled in old heat exchangers during maintenance operations to enhance the heat transfer in these heat exchangers.

– A correlation has been developed to represent the relation between heat transfer and friction for the case of shell and tube heat exchanger with multi inserted swirl vanes.

References

[1] C. Liang, G. Papadakis, Large eddy simulation of cross-flow through a staggered tube bundle at subcritical Reynolds number, J. Fluids Struct. 23 (2007) 1215–1230.

[2] T. Sobota, Experimental prediction of heat transfer correlations in heat exchangers, in: M.A.S. Bernades (Ed.), Development in Heat Transfer, In-Tech, Vienna – Rijeka, 2011. Cracow University of Technology, Poland, Chapter 16, ISBN 978-953-307-569-3.

[3] M.G. Yehia, A.A.A. Attia, O.S. Abdelatif, E.E. Khalil, Computational investigations of thermal simulation of shell and tube heat exchanger, in: Proceedings of the ASME 2014 12th Biennial Conference on Engineering Systems Design and Analysis, ESDA2014, Copenhagen, Denmark, June 25–27, 2014.

[4] M.G. Yehia, A.A.A. Attia, O.S. Abdelatif, E.E. Khalil, On the computations of thermal behavior of shell and tube heat exchanger, in: Proceedings of the AIAA Propulsion and Energy Forum and Expositions 2014, Cleveland, Ohio, USA, July 28–30, 2014.

[5] I. Kurtbas, A. Durmus, H. Eren, E. Turgut, Effect of propeller type swirl generators on the entropy generation and efficiency of heat exchangers, Int. J. Therm. Sci. 46 (3) (2007) 300–307.

[6] S. Eiamsa-ard, C. Thianpong, P. Eiamsa-ard, P. Promvonge, Thermal characteristics in a heat exchanger tube fitted with dual twisted tape elements in tandem, J. Int. Commun. Heat Mass Transfer 37 (1) (2010) 39–46.

[7] C. Thianpong, P. Eiamsa-ard, K. Wongcharee, S. Eiamsa-ard, Compound heat transfer enhancement of a dimpled tube with a twisted tape swirl generator, J. Int. Commun. Heat Mass Transfer 36 (2009) (2009) 698–704.

[8] H.Z. Blasius, The Law of Similar Procedures in Liquids Friction, Researchers Arb. Ing. Wes. 131, Berlin, 1913.

[9] B.S. Petukhov, Heat transfer and friction in turbulent pipe flow with variable physical properties, in: T.F. Irvine, J.P. Hartnett (Eds.), Advances in Heat Transfer, vol. 6, Academic Press, New York, 1970.

[10] A.P. Colburn, A method of correlating forced convection heat transfer data and a comparison with liquid friction", Trans. Am. Inst. Chem. Eng. 29 (1933) 174–210.

[11] R.H.S. Winterton, Where did the Dittus and Boelter equation come from?, Int J. Heat Mass Transfer 41 (4–5) (1998) 809–810.

[12] K.J. Bell, Final Report of the Cooperative Research Program on Shell and Tube Heat Exchangers, Bull. No. 5, University of Delaware Engineering Experiment Station, New York, 1963.

[13] D.D. Col, A. Muzzolon, P. Piubello, L. Rosetto, Measurement and prediction of evaporator shell-side pressure drop, Int. J. Refrig. 28 (2005) 320–330.

[14] E. Ozden, I. Tari, Shell side CFD analysis of a small shell-and-tube heat exchanger, J. Energy Convers. Manage. 51 (2010) 1004–1014.

[15] U. Ur-Rehman, Heat Transfer Optimization of Shell-and-Tube Heat Exchanger through CFD Studies M.Sc. Thesis, Chalmers University of Technology, Göteborg, Sweden, 2011.

[16] ANSYS Fluent Documentation, ANSYS Inc, Release 15.0, 2013.

[17] F.P. Incropera, D.P. DeWitt, T.L. Bergman, A.S. Lavine, Introduction to Heat Transfer, sixth ed., John Wiley & Sons Inc., 2011.

[18] S. Eiamsa-ard, P. Promvonge, Experimental investigation of heat transfer and friction characteristics in a circular tube fitted with V-nozzle turbulators, J. Int. Commun. Heat Mass Transfer 33 (5) (2006) 591–600.